

Generalizing the first-difference correlated random walk for marine animal movement data

Christoffer Moesgaard Albertsen

National Institute of Aquatic Resources, Technical University of Denmark,

Kemitorvet 201, DK-2800 Kgs. Lyngby, Denmark

cmoe@aqua.dtu.dk

Abstract

Animal telemetry data are often analysed with discrete time movement models assuming rotation in the movement. These models are defined with equidistant distant time steps. However, telemetry data from marine animals are observed irregularly. To account for irregular data, a time-irregularised first-difference correlated random walk model with drift is introduced. The model generalizes the commonly used first-difference correlated random walk with regular time steps by allowing irregular time steps, including a drift term, and by allowing different autocorrelation in the two coordinates. The model is applied to data from a ringed seal collected through the Argos satellite system, and is compared to related movement models through simulations. Accounting for irregular data in the movement model results in accurate parameter estimates and

reconstruction of movement paths. Measured by distance, the introduced model can provide more accurate movement paths than the regular time counterpart. Extracting accurate movement paths from uncertain telemetry data is important for evaluating space use patterns for marine animals, which in turn is crucial for management. Further, handling irregular data directly in the movement model allows efficient simultaneous analysis of several animals.

Key words: animal telemetry, movement ecology, correlated random walk, irregular data

Introduction

Understanding animal movement behaviour, space use patterns and response to the environment relies on modelling animal telemetry data. So far, the collection of telemetry data has been hindered in marine environments. Satellite systems require animals to surface, storage tags require recapture, and acoustic networks require a dense array of receivers. Nonetheless, the scope and scales of movement studies are continuously increasing with rapid technological advances in tracking devices ([Hussey et al., 2015](#)).

In spite of technological advances leading to more accurate measurements and larger data sets, data from satellite tags have inherent measurement errors. Systems such as Fastloc GPS and Argos can only record data when the animal is above water, with an accuracy that depends on the surface time and diving behaviour ([Costa et al., 2010](#)). Typically, this results in data observed at irregular time steps with considerable uncertainty, which makes state-space models a valuable framework for analysing the data.

State-space models naturally separate the movement process from measurement errors. True animal locations are explicitly modelled separately from the observed measurements conditionally on the locations. Hence, the movement models developed can be combined with telemetry data from any source, for example, GPS, Argos, light based, or acoustic tags. However, inference in general state-space models can be challenging. Maximum likelihood estimation in state-space models requires integration of the joint distribution of locations and measurements over the locations to obtain the marginal distribution of the observations. Recent software such as AD Model Builder ([Fournier et al., 2012](#)) and Template Model Builder (TMB; [Kristensen et al., 2016](#)) utilizes the Laplace approximation to rapidly approximate the marginal distribution of observations in state-space models. While care is needed to ensure the approximation is appropriate, this framework is generally applicable. For instance, TMB has been used for both discrete time ([Auger-Méthé et al., 2016, 2017](#)) and continuous time ([Albertsen et al., 2015](#)) movement models. Alternatively, the state-space can be discretized and the resulting hidden Markov model can be used for inference ([Pedersen et al., 2011](#)).

Although continuous time movement models can handle irregular data, discrete time models are often thought of as more intuitive ([McClintock et al., 2014](#)). Further, continuous time models can be difficult to construct or extend analytically, because they are often formulated through stochastic differential equations. Whereas continuous time models describe instantaneous change, discrete time models describe the change between two observations. In animal movement models, the change between observations are often modelled through a step length and an angle of movement (e.g., [Morales et al., 2004](#); [Jonsen et al., 2005](#); [Gurarie et al., 2009](#); [Tracey et al., 2010](#); [McClintock et al., 2012](#); [Michelot et al., 2016](#)), which is considered a natural way to represent movement ([Turchin, 1998](#)). In discrete time models

with regular time steps, irregular data can be handled by modifying the observational model to interpolate between states ([Jonsen et al., 2005](#)).

To facilitate the analysis of populations or meta-analysis of individuals, the model parameters for different individuals must be on the same scale. If the interpretation of parameter values depends on the chosen time steps between estimated locations ([McClintock et al., 2014](#)), the values must be corrected before comparison is possible. Likewise, estimating population parameters based on individuals either requires movement models that use the same time steps for all individuals (e.g. [Jonsen, 2016](#)), which can be sub-optimal, or movement models that handle irregular data directly.

The first-difference correlated random walk (DCRW; [Jonsen et al., 2005](#)) models the animal movement as a discrete time first order auto-regressive process on the difference between consecutive locations through a rotation matrix. A continuous time version of the DCRW without rotation is the continuous time correlated random walk (CTCRW; [Johnson et al., 2008](#)). The CTCRW models the velocity of an animal by an Ornstein-Uhlenbeck process: the continuous time counterpart of the first order auto-regressive process. Recently, an irregular time version of the DCRW was introduced without rotation including a time-varying parameter instead ([Auger-Méthé et al., 2017](#)).

In this paper, a generalization of the DCRW is introduced. The generalization of the DCRW is trifold: the model allows irregular time steps, a drift vector is included, and different auto-correlations in the two coordinates can be used. As a by-product, it is shown how parameters of the DCRW model depends on the selected time steps, and how to transform them to a common scale. The generalized DCRW is introduced as the discretization of a stochastic differential equation for the animal's velocity and location. Further, the close

relation to a generalization of the CTCRW is shown. Through three simulation studies, the generalized DCRW is shown to perform well compared to the CTCRW and DCRW. Finally, The applicability and extendability of the model is illustrated through a real data set collected by the Argos system.

Materials and Methods

Movement model

The generalization of the DCRW movement model is constructed through a stochastic differential equation (SDE) for the velocity. From this SDE, the location process is the integrated velocity process. To obtain the time-irregular movement model, the SDE is solved analytically while the location process is a discrete time approximation.

SDE for velocity

The bivariate SDE for the velocity, V_t , of an animal is

$$\begin{aligned} dV_t &= - \begin{pmatrix} -\log \gamma_1 & \theta \\ -\theta & -\log \gamma_2 \end{pmatrix} (V_t - \mu)dt + SdB_t \\ &= -\Theta(V_t - \mu)dt + SdB_t \end{aligned} \tag{1}$$

with initial condition $V_0 = v_0 \in \mathbb{R}^2$. In this model, γ_1 and γ_2 are autocorrelation parameters, μ is a vector of mean velocity parameters, and θ is the mean turning angle of the movement process. The matrix S is a lower triangular matrix with positive diagonal determining the

covariance of the changes in velocity. Animals moving persistently in one direction will have high autocorrelation in the velocity and a mean turning angle close to zero, while animals foraging or in other ways displaying a tortuous movement will have a lower autocorrelation in the velocity and a mean turning angle different from zero (modulo 2π) (e.g. [Jonsen et al., 2005](#); [Whoriskey et al., 2017](#)).

The analytical solution to the SDE is a stochastic process with Gaussian increments (see e.g. Supplemental Material). The mean of an increment is

$$E(V_t | V_s) = \exp(-\Theta(t-s))V_s + (I - e^{-\Theta(t-s)})\mu, \quad s < t$$

where $\mu = (\mu_1, \mu_2)^T$, while the covariance is

$$\text{vec}(\text{Var}(V_t | V_s)) = \text{vec}(C) - e^{-\Theta(t-s)} \otimes e^{-\Theta(t-s)} \text{vec}(C), \quad s < t$$

where $\text{vec}(C) = (\Theta \oplus \Theta)^{-1} \text{vec}(\Sigma)$, $\Sigma = SS^T$, \oplus denotes the Kronecker sum, $A \oplus B = A \otimes I_B + I_A \otimes B$, and vec is an operator that stacks the columns of a matrix to a vector.

Based on the velocity, the location process, X_t , follows the SDE

$$dX_t = V_t dt \tag{2}$$

Discretizing the SDE for locations

Considering the N predetermined time points $\{t_i\}_{i \in \{1, \dots, N\}}$, an Euler–Maruyama approximation to the location process is obtained by

$$X_{t_i} = X_{t_{i-1}} + V_{t_{i-1}} \Delta_i$$

where $\Delta_i = t_i - t_{i-1}$ is the length of the time step. Inserting the expression for $V_{t_{i-1}}$, the Generalized first-Differenced Correlated Random Walk (GDCRW) is obtained:

$$X_{t_i} = X_{t_{i-1}} + \Delta_i \exp(-\Theta \Delta_{i-1})(X_{t_{i-1}} - X_{t_{i-2}})/\Delta_{i-1} + \Delta_i (I - \exp(-\Theta \Delta_{i-1})) \mu + \Delta_i \epsilon_{t_i} \quad (3)$$

The error terms, ϵ_{t_i} , follow a zero mean normal distribution with variance

$$\text{Var}(\epsilon_{t_i}) = C - \exp(-\Theta \Delta_i) C \exp(-\Theta^T \Delta_i)$$

where

$$\text{vec}(C) = (\Theta \oplus \Theta)^{-1} \text{vec}(\Sigma),$$

and $\Sigma = SS^T$ is a covariance matrix.

Special cases

The GDCRW model is closely related to four other models: The CTCRW, the DCRW, the modified DCRW by [Auger-Méthé et al. \(2017\)](#), and a random walk.

Relation to the CTCRW When the turning-angle parameter $\theta = 0$, and the increment covariance S is diagonal, the velocity model, V_t is identical to the velocity model of the CTCRW; however, the location models differ. While the location model of the CTCRW is an analytical solution to the two univariate integrated velocity models, the GDCRW is a discretization of the more general bivariate velocity model. Hence, when the length of the time steps approaches zero, the GDCRW approaches the CTCRW when the velocity models are identical. When $\theta \neq 0$ or S is not diagonal, the GDCRW approaches a generalization of the CTCRW when the length of the time steps approaches zero.

Relation to the DCRW For regularly observed data, $\Delta_t = \Delta$, with $\mu = 0$ and $\gamma_1 = \gamma_2$,

$$\exp(-\Theta\Delta) = \begin{pmatrix} \cos(\theta\Delta) & -\sin(\theta\Delta) \\ \sin(\theta\Delta) & \cos(\theta\Delta) \end{pmatrix} \gamma^\Delta$$

Hence, the movement model simplifies to

$$X_i = X_{i-1} + \begin{pmatrix} \cos(\theta\Delta) & -\sin(\theta\Delta) \\ \sin(\theta\Delta) & \cos(\theta\Delta) \end{pmatrix} \gamma^\Delta (X_{i-1} - X_{i-2}) + \Delta\epsilon_i, \quad (4)$$

which is the movement model of [Jonsen et al. \(2005\)](#) when $\Delta = 1$. Therefore, the GDCRW generalizes the DCRW in three ways: the restriction of regular time steps is relaxed, a drift vector is added, and different auto-correlations in the two coordinates are allowed. Further, equation (4) allows scaling the DCRW parameters to a common time scale. That is, if parameters $\tilde{\gamma}$ and $\tilde{\theta}$ are obtained from a DCRW model fitted with time steps $\tilde{\Delta}$, scale independent parameters are obtained by $\gamma = \tilde{\gamma}^{1/\tilde{\Delta}}$ and $\theta = \tilde{\theta}/\tilde{\Delta}$. Being able to scale the

DCRW parameters to a common scale allows comparison between model fits in meta or population studies even if different time scales are used.

Relation to the modified DCRW Recently, [Auger-Méthé et al. \(2017\)](#) proposed a modified version of the DCRW for Fastloc-GPS data. The modified DCRW allowed irregularly observed data and included a time-varying autocorrelation parameter, γ_t . Ignoring the time-varying autocorrelation, the modified DCRW can be obtained as a special case of the GDCRW introduced here by letting $\gamma_1 = \gamma_2 = \gamma_t$, $\mu = 0$, $\theta = 0$, and by letting Σ be a diagonal matrix. Note, however, that the two models differ slightly in parameterization. In the modified DCRW, γ_t is not scaled by the time differences and the variance of ϵ_{t_i} is parameterized as a diagonal matrix $diag(\sigma_1^2, \sigma_2^2)$. The GDCRW can easily be extended to have a time-varying autocorrelation parameter in the same way as [Auger-Méthé et al. \(2017\)](#).

Relation to a random walk In the same manner as the three models above, the GDCRW can be reduced to a random walk model. From equation (3) it follows that when the autocorrelation parameters γ_1 and γ_2 tend to zero, the model is reduced to a random walk. If $\mu \neq 0$, it will be a random walk with drift.

Measurement equation

Besides the movement process describing the latent states, $\{X_{t_i}\}_{i \in \{1, \dots, N\}}$, a measurement equation is needed to form a state-space model. For the DCRW, measurement errors are often included by linearly interpolating between the latent states. For an observation Y_{s_j} at

time s_j ,

$$Y_{s_j} = (1 - q)X_{t_i} + qX_{t_{i+1}} + \eta_j$$

such that $t_i \leq s_j < t_{i+1}$, $q = \frac{s_j - t_i}{\Delta_{i+1}}$, and η_i is a zero mean bivariate random variable. However, when the movement model allows irregular time steps, it is more natural to ensure that the latent states align with the observations, such that the measurement equation simplifies to

$$Y_{s_j} = X_{s_j} + \eta_j$$

Then the observation at time s_j does not depend on a latent state in the future. Note that the state-space model can include additional latent states between observations. These latent states only contributes to the likelihood function through the movement process. Below, η_j will either be modelled as a bivariate normal distribution ([Johnson et al., 2008](#)) or a bivariate t-distribution ([Albertsen et al., 2015](#)).

Simulation study: Comparing the GDCRW and the CTCRW

Since the location process is constructed as an Euler–Maruyama discrete time approximation to an underlying continuous time model, increasing the number of latent states between observations should improve the approximation. This was investigated by simulating from the underlying continuous time model in the special case that reduces to the CTCRW. On each simulated data set, the CTCRW was compared to the GDCRW with latent states at the observations, and the GDCRW_{*i*} with additional latent states every $i = 8, 4, 2$, and 1 time unit, respectively.

To compare the GDCRW with the CTCRW, 200 data sets were simulated from the continuous time model defined by equations (1) and (2) with $\theta = 0$ and diagonal S ; that is, with the CTCRW as the true model. To obtain locations, 250 time steps were simulated from a mixture of an exponential and a normal distribution (see Supplemental Material) to ensure both short and long time steps between observations. Between the simulated time points, the velocity and location processes were simulated using the Euler–Maruyama method with 200 steps. For each of the 250 simulated locations, observations were simulated from a bivariate normal with covariance $0.1^2 I$. The processes were simulated with $\gamma_1 = \gamma_2 = 0.9$, $\mu = 0$, and $S_{11} = S_{22} = \exp(-2) \approx 0.135$. The models were fitted to the data by maximum likelihood through the Laplace approximation using the R package TMB (Kristensen et al., 2016). For simplicity, the model was fitted with $\gamma_1 = \gamma_2$, $\theta = 0$, $\mu = 0$, and $S_{12} = S_{21} = 0$.

Simulation study: Comparing the GDCRW and the DCRW

Above it was established that the DCRW was a special case of the GDCRW. One of the ways the DCRW was generalized was that the GDCRW allowed latent states at arbitrary time points. In contrast, the DCRW only allowed equidistant time steps in discretizing the underlying SDE. In this simulation study the effect of the choice of discretization on parameter estimates was investigated.

Data sets were simulated from two behavioural scenarios using the same procedure as for the previous simulation study. For each scenario, 200 data sets were simulated from the continuous time model determined by equations (1) and (2). The first scenario emulated tortuous movement simulated with $\phi = \frac{\pi}{3} \approx 1.05$, $\mu = 0$, and $\gamma_1 = \gamma_2 = 0.6$. The movement

was simulated with diagonal S such that $S_{11} = S_{22} = \exp(-2)$. Measurements were simulated from a normal distribution with covariance $\Sigma_o = 0.1^2 I_2$. The second scenario mimicked a more persistent movement. Movement was simulated with $\phi = 0$ and $\gamma = 0.7$. Similar to the first scenario, the movement was simulated with $S_{11} = S_{22} = \exp(-2)$ and the observations with $\Sigma_o = 0.1^2 I_2$.

For each data set, a total of 10 models were fitted consisting of the GDCRW and the DCRW with $N = 250, 500, 750, 1000,$ and 1250 latent locations. In the DCRW, the latent locations were included equidistantly. In the GDCRW, 250 latent locations were aligned with the observations. Remaining latent locations were included recursively in the middle of the longest time step. The models were fitted to the data by maximum likelihood through the Laplace approximation. For simplicity, the DCRW models were fitted with $S_{11} = S_{22}$, and $S_{12} = S_{21} = 0$. The GDCRW models were fitted with $\gamma_1 = \gamma_2$, $\mu = 0$, $S_{11} = S_{22}$, and $S_{12} = S_{21} = 0$ to reduce to the same parameters as the DCRW models.

Simulation study: Effect of measurement error on choice of time steps

In the final simulation study, the GDCRW and DCRW is compared once more. While the previous comparison focused on parameter estimates, this simulation study compares the ability to accurately obtain location estimates for different ratios of process variability and measurement variability. Again, 200 data sets with 250 observations were simulated from two behavioural scenarios using the same procedure as for the two previous simulation studies. The same movement parameters as in the previous simulation study was used, and the GDCRW

and DCRW with 250 latent locations were fitted in the same manner as before; however, the observations were simulated with covariances $\exp(-6)^2 I, \exp(-5.5)^2 I, \dots, \exp(1.5)^2 I, \exp(2)^2 I$, respectively. For each location for each track the relative distance to the true locations were calculated for the GDCRW compared to the DCRW. The DCRW locations were interpolated linearly to get values at the time of observations.

Case study: Ringed seal

To illustrate its practical applicability, the GDCRW model was fitted to the subadult ringed seal *Pusa hispida* data of [Albertsen et al. \(2015\)](#) in this case study. The data set was chosen to illustrate the movement model when substantial measurement errors are present. The ringed seal data consists of $N = 3583$ locations collected by the Argos satellite system, which is known to have substantial non-Gaussian measurement errors. Three observations with location class Z were excluded. In the first period of the track, the seal was moving north-west, followed by two periods with restricted space use close to land. Consequently, [Thygesen et al. \(2017\)](#) found indications that a non-constant drift parameter was needed. To account for this behaviour, the mean velocity parameters of the GDCRW were set to be location dependent:

$$X_{t_i} = X_{t_{i-1}} + \Delta_{t_i} \exp \left(- \begin{pmatrix} -\log \gamma_1 & \theta \\ -\theta & -\log \gamma_2 \end{pmatrix} \Delta_{t_{i-1}} \right) (X_{t_{i-1}} - X_{t_{i-2}}) / \Delta_{t_{i-1}} \\ + \Delta_{t_i} \left(I - \exp(-\Theta \Delta_{t_{i-1}}) \right) \mu(X_{t_{i-1}}) + \Delta_{t_i} \epsilon_{t_i}$$

The bivariate mean velocity field $\mu(X_t) = (\mu_1(X_t), \mu_2(X_t))^T$ was modelled through a 7×7 grid of random effects. Each grid point was related to two random effects: one for the mean latitudinal velocity, μ_1 , and one for the mean longitudinal velocity, μ_2 . Between the grid points, the random effect values were interpolated by a search tree approximation to local polynomial regression (Albertsen, 2017). In this case study, the number of random effects to construct the grids were selected as a trade-off between computational cost and flexibility. Locations of the movement process were estimated at every observation and every three hours from the first observation, giving a total of 4764 location estimates each with two latent states. Following Albertsen et al. (2015), the measurements were modelled by a bivariate t-distribution with scale matrices and degrees of freedom depending on the location class of the observations. The model was fitted to the data by maximum likelihood through the Laplace approximation using TMB.

Having a location dependent drift in the model, the animal movement may be related to available resources or hydrographic variables. The model cannot be estimated using the DCRW, since the DCRW does not include a drift parameter. Furthermore, the model cannot easily be estimated using CTCRW without assuming constant movement between states, in which case the CTCRW is a special case of the GDCRW (see [Relation to the CTCRW](#)).

Results

Simulation study: Comparing the GDCRW and the CTCRW

In the first simulation study, the GDCRW was compared to the CTCRW, when the CTCRW was the true data generating model. The CTCRW models both the velocity and location giving a total of 1000 latent variables: 4 for each location. In contrast, the GDCRW only has 500 latent variables: 2 for each location. The mean of the time step distribution used in the simulation study was approximately 1.99, giving an average length of a simulated trajectory of 497.5 time units. Therefore, the GDCRW₈ would include 63 additional location estimates on average, corresponding to a total of 313 latent variables. Likewise, the GDCRW₄, GDCRW₂, and GDCRW₁ would on average include 125, 249, and 498 additional locations, respectively, corresponding to 750, 998, and 1496 latent variables.

Regardless of the different number of latent variables, all six estimation models provided γ estimates close to the true value (Fig. 1). For the true continuous time model, the CTCRW, the average of the 200 estimates was 0.894, whereas it was 0.897 for the discrete time approximation, the GDCRW, with latent states only at the time of the observations. When additional latent states were included every 8, 4, 2, and 1 time unit, the average of the estimated γ s were 0.901, 0.903, 0.9, and 0.897, respectively. Although all models gave estimates close to the true value, the standard deviation of the estimates was higher for the GDCRW than for the five other models. For the GDCRW the standard deviation of the 200 estimates was 0.028, whereas it was 0.019 for the CTCRW, and 0.018, 0.017, 0.017, and 0.018 for the GDCRW₈, GDCRW₄, GDCRW₂, and GDCRW₁, respectively.

Besides the ability to re-obtain the true parameters, the models were compared on the

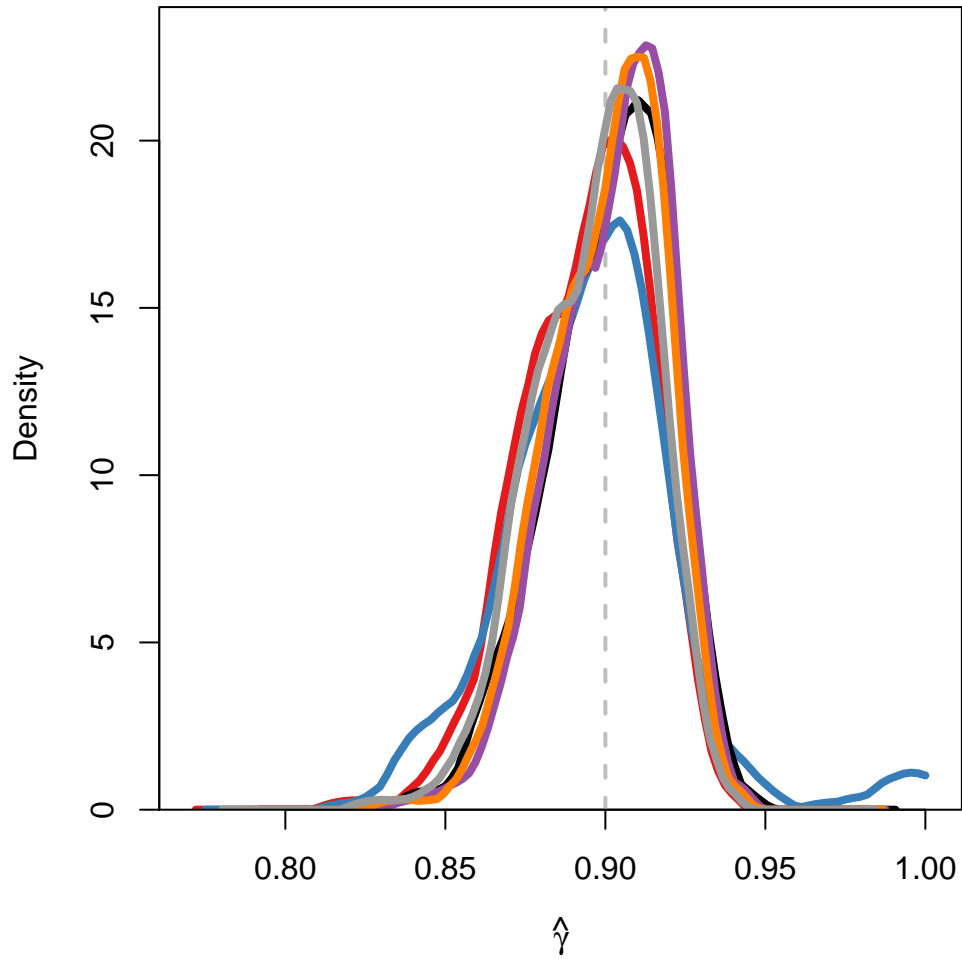


Fig. 1: Density of γ estimates in the simulation study for the models: CTCRW (red line), GDCRW (blue line), GDCRW₈ (black line), GDCRW₄ (purple line), GDCRW₂ (orange line), and GDCRW₁ (grey line). Grey dashed line indicates the true parameter value.

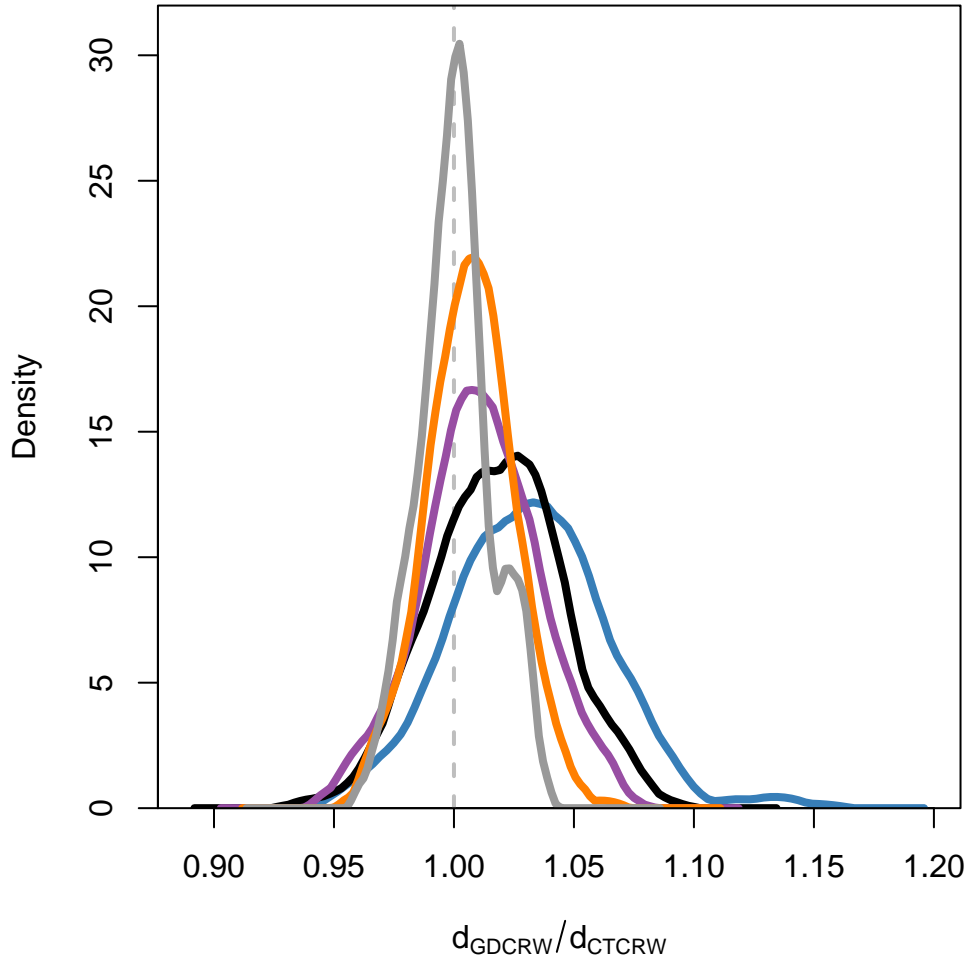


Fig. 2: Density of track-wise median distance between estimated locations and true simulated locations in the simulation study for the models: GDCRW (blue line), GDCRW₈ (black line), GDCRW₄ (purple line), GDCRW₂ (orange line), and GDCRW₁ (grey line) relative to the CTCRW. A value of one (grey dashed line) indicates the median distance is the same as for the CTCRW.

distance between the estimated locations and the true simulated locations [Fig. 2](#). To compare the models, this distance was calculated for each location for each track for the GDCRW, GDCRW₈, GDCRW₄, GDCRW₂, and GDCRW₁, and divided by the distance obtained for the CTCRW. Finally, the median relative distance was obtained. Whereas the models performed similarly in estimating γ , the CTCRW performed better than the other models in obtaining precise location estimates; however, the GDCRW models improved when additional latent states were included, as expected. For the GDCRW, 16% of the simulations had a relative distance compared to the CTCRW that was less than one; that is, where at least half of the estimated locations were closer to the true location than for the estimated locations from the CTCRW. For the GDCRW₈, 24% of the simulations had a relative distance less than one, while it was 31, 36, and 47%, respectively, for the GDCRW₄, GDCRW₂, and GDCRW₁. Further, the range of median relative distances narrowed when the number of latent states increased. When no additional latent states were included, the length of the range was 0.188 (0.958;1.146). Based on these 200 simulations, the range gradually narrowed for the GDCRW₈ (0.143; min: 0.958; max: 1.146), GDCRW₄ (0.116; min: 0.953; max: 1.069), GDCRW₂ (0.099; min: 0.962; max: 1.061), and GDCRW₁ (0.072; min: 0.964; max: 1.036).

Simulation study: Comparing the GDCRW and the DCRW

In the second simulation study, the parameter estimates from the GDCRW and DCRW were compared in two movement scenarios. In the tortuous movement scenario, the GDCRW provided γ estimates close to the true value for all five number of latent locations with a slight tendency to overestimate the value ([Fig. 3](#)). The average γ estimates (standard deviation)

were 0.622 (0.059), 0.643 (0.061), 0.625 (0.062), 0.614 (0.066), and 0.611 (0.067) for the GDCRW with $N = 250, 500, 750, 1000,$ and 1250 latent locations, respectively. A difference was, however, seen in for the θ estimates. Their accuracy increased with the number of latent locations. The average estimates were 0.729 (0.139), 0.956 (0.124), 0.999 (0.124), 1.028 (0.129), and 1.033 (0.134), respectively. Unlike for the GDCRW, the estimates obtained directly from the DCRW were not close to the true values. For these models, the average γ estimates were 0.56 (0.067), 0.654 (0.061), 0.734 (0.053), 0.787 (0.046), and 0.823 (0.041) with $N = 250, 500, 750, 1000,$ and 1250 latent locations, respectively, while the average θ estimates were 1.841 (0.237), 1.059 (0.178), 0.705 (0.124), 0.528 (0.094), and 0.427 (0.113). Correcting the estimates obtained from the DCRW by equation (4), the accuracy of the estimates increased with the number of latent locations. Then, the average γ estimates were 0.746 (0.046), 0.653 (0.059), 0.63 (0.064), 0.621 (0.066), and 0.616 (0.069), respectively, while the average θ estimates were 0.921 (0.114), 1.057 (0.133), 1.055 (0.136), 1.054 (0.138), and 1.066 (0.241).

In the persistent movement scenario, the GDCRW and the DCRW corrected by equation (4) provided estimates close to the true values for both parameters for all five number of latent locations (Fig. 4). For the GDCRW, the average γ estimates were 0.897 (0.028), 0.897 (0.028), 0.899 (0.019), 0.897 (0.019), and 0.896 (0.019), respectively, and the average θ estimates were 0.002 (0.02), 0.002 (0.02), 0.002 (0.019), 0.002 (0.019), and 0.002 (0.019). Likewise, the average DCRW estimates corrected by equation (4) were 0.9 (0.019), 0.898 (0.019), 0.898 (0.019), 0.897 (0.019), and 0.897 (0.019), respectively, for γ , and 0.002 (0.019), 0.002 (0.019), 0.002 (0.019), 0.002 (0.019), and 0.002 (0.019), respectively, for θ . Similarly to the tortuous movement scenario, the estimates obtained directly from the DCRW were not close to the

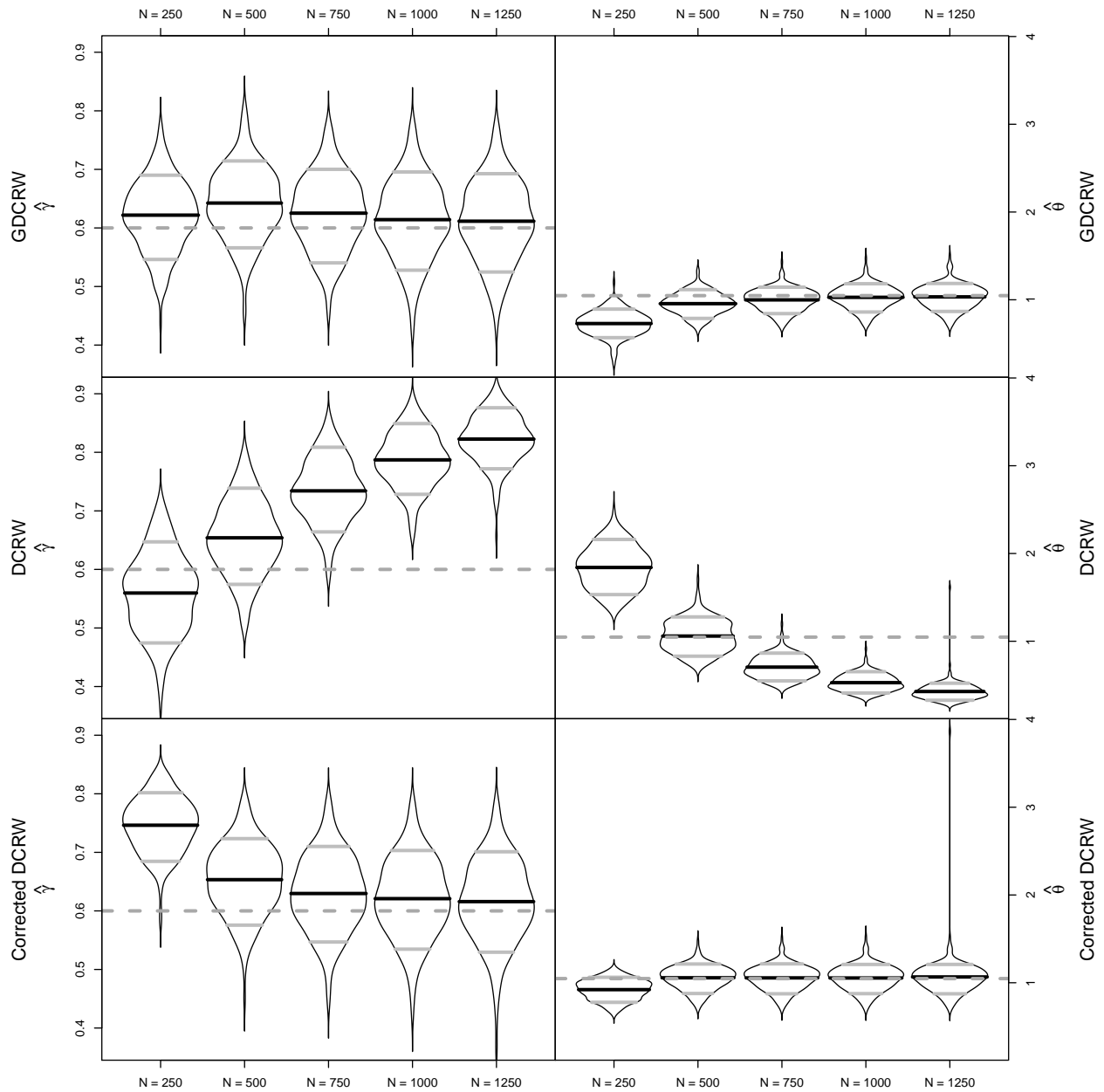


Fig. 3: Violin plots of γ and θ estimates in the tortuous movement simulations for the GDCRW, DCRW, and the DCRW corrected by equation (4) with $N = 250, 500, 750, 1000, 1250$ latent states and 250 observations. Grey dashed lines indicate true parameter values. In the violin plot, black lines indicate the mean of estimates and grey lines indicate 10 and 90 % quantiles of estimates.

true values. For the DCRW models, the average γ estimates were 0.812 (0.037), 0.898 (0.022), 0.931 (0.015), 0.948 (0.011), and 0.958 (0.009) with $N = 250, 500, 750, 1000,$ and 1250 latent locations, respectively, while the average θ estimates were 0.003 (0.038), 0.002 (0.019), 0.001 (0.012), 0.001 (0.009), and 0.001 (0.007).

Simulation study: Effect of measurement error on choice of time steps

In the third simulation study, the GDCRW and DCRW were compared again. This simulation study compared location estimates for different levels of measurement error. When the measurement standard deviation was low, the GDCRW performed notably better than the DCRW (Fig. 5). In both scenarios, all 200 simulations had a median relative distance less than 1; that is, at least half of the locations were better estimated by the GDCRW than the DCRW. As the measurement standard deviation increases relative to the movement standard deviation, the median relative distance tends to one, suggesting that the GDCRW and the DCRW estimates similarly. When the measurement and movement standard deviation were equal, the DCRW performed slightly better than the GDCRW.

Case study: Ringed seal

In the case study, the GDCRW was fitted to a real data set collected by the Argos system. The GDCRW was modified to include location dependent drift and turning angle. The fitted model resulted in small estimated longitudinal mean velocity field values (Fig. 6). On the contrary, the latitudinal mean velocity field was estimated to have a southward drift when

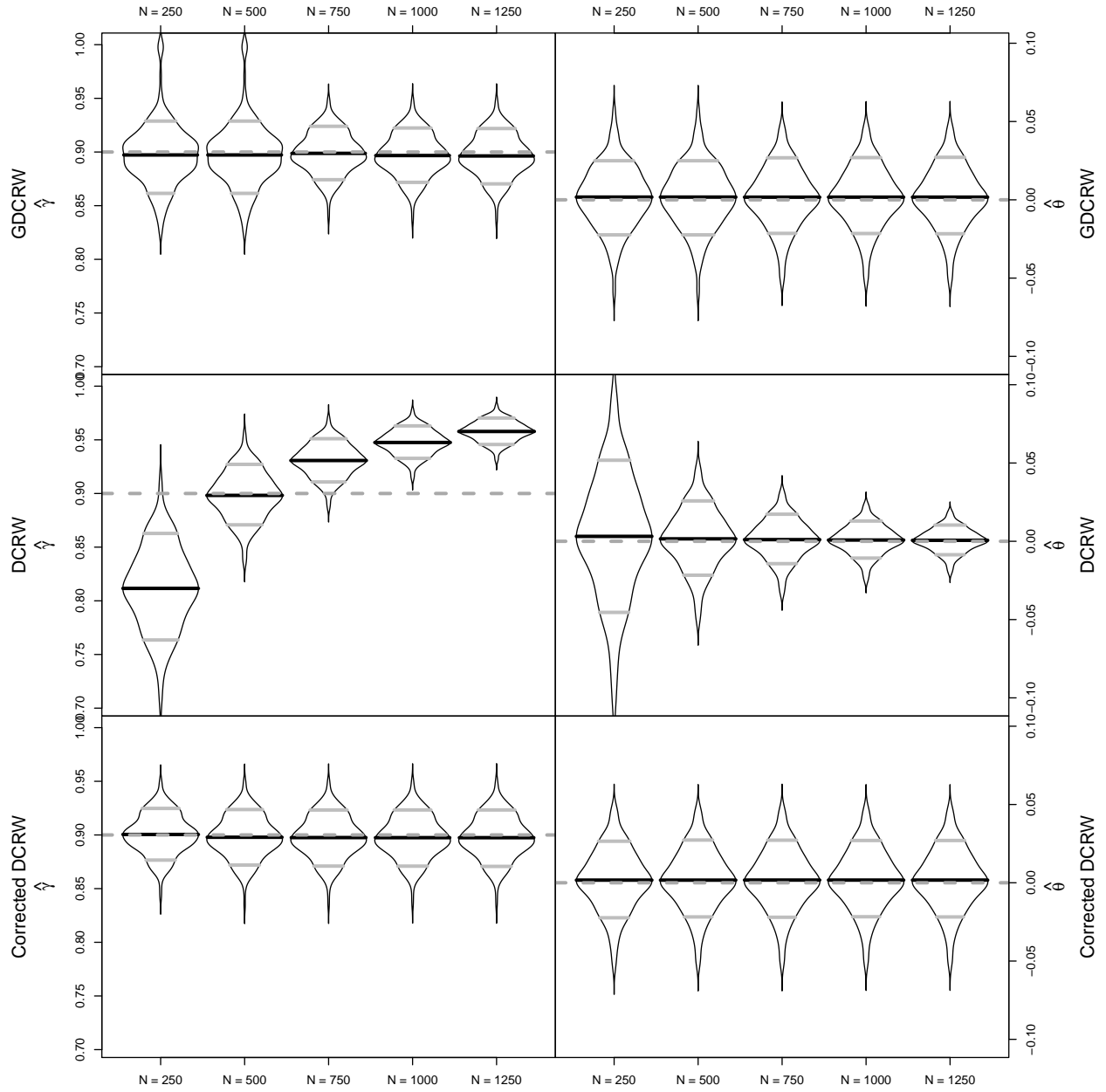


Fig. 4: Violin plots of γ and θ estimates in the persistent movement simulations for the GDCRW, DCRW, and the DCRW corrected by equation (4) with $N = 250, 500, 750, 1000, 1250$ latent states and 250 observations. Grey dashed lines indicate true parameter values. In the violin plot, black lines indicate the mean of estimates and grey lines indicate 10 and 90 % quantiles of estimates.

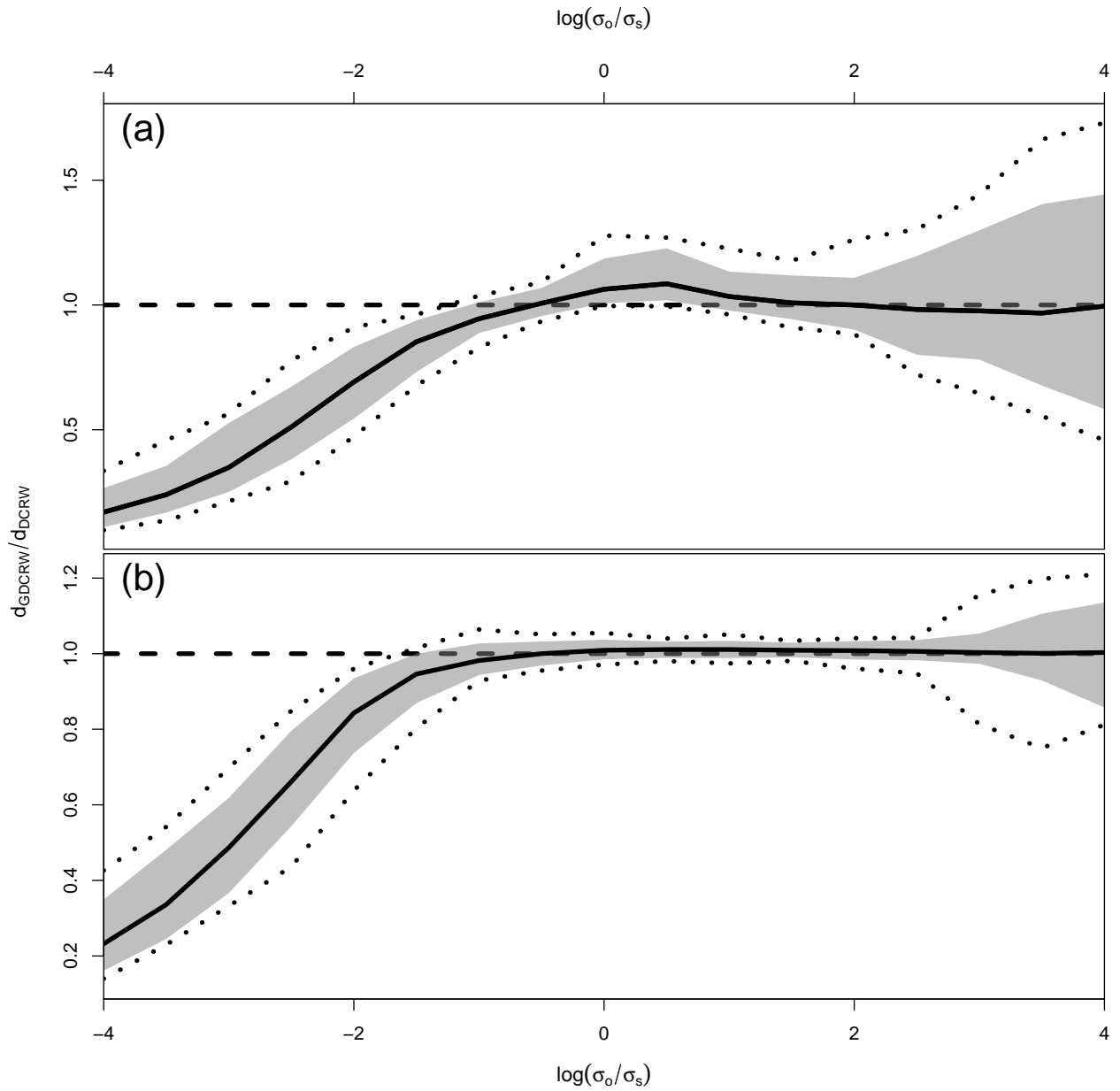


Fig. 5: Minimum (lower dotted black line), maximum (upper dotted black line), median (full black line), and 95% range (grey area) of track-wise median distances between estimated locations and true simulated locations for the GDCRW relative to the DCRW in the tortuous (a) and persistent (b) simulated movement scenarios as a function of the ratio between observational standard deviation (σ_o) and movement standard deviation (σ_s). Values below 1 (black dashed line) indicates that at least half of the estimated location in the GDCRW were closer to the true value than for the DCRW.

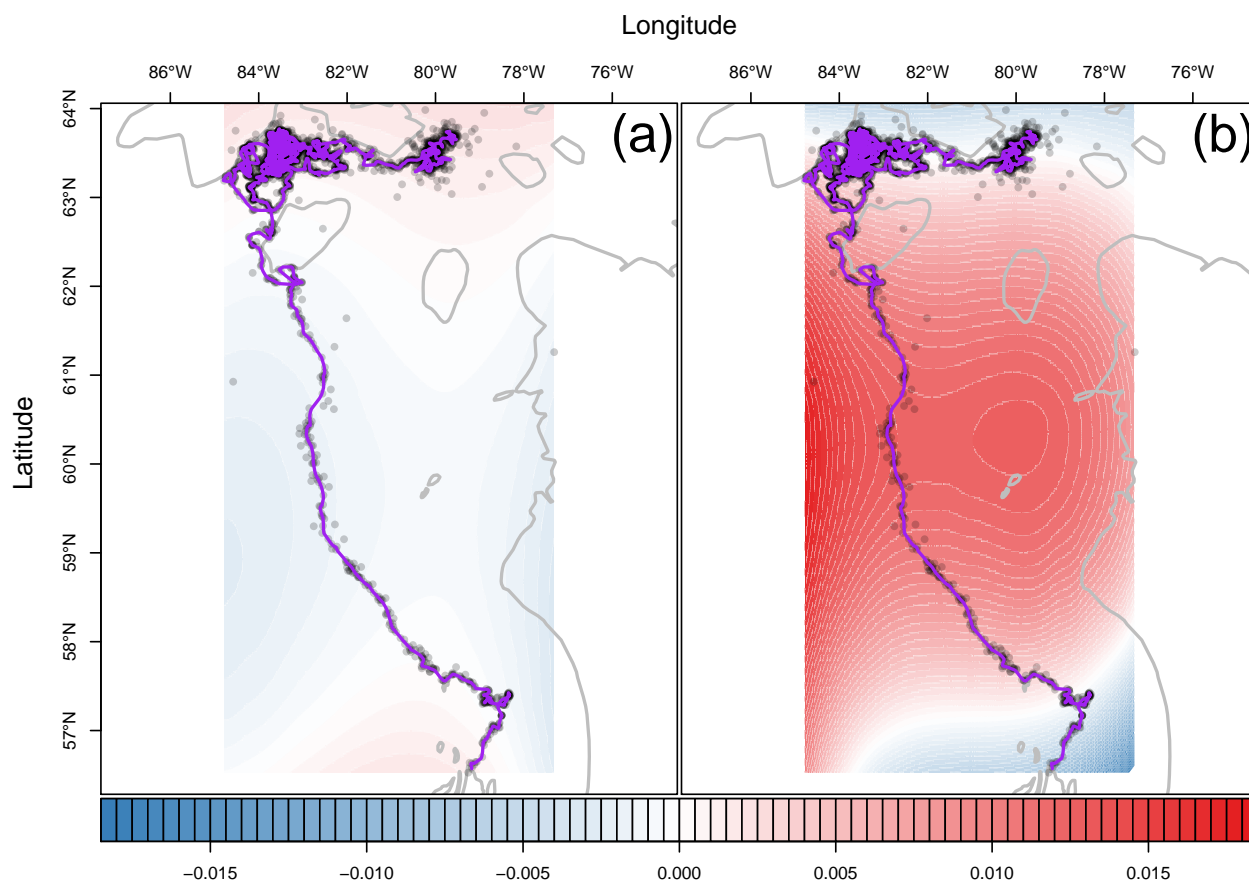


Fig. 6: Mean longitudinal (a) and latitudinal (b) velocity field of the subadult ringed seal track with land (outlined by grey lines), Argos satellite observations (dark grey dots), and fitted most probable track given all observations (purple line). In the longitudinal field, red values indicate an eastward attraction, while blue values indicate a westward attraction. In the latitudinal field, red values indicate a northward attraction, while blue values indicate a southward attraction.

Table 1: Estimated movement parameters in the ringed seal case study.

	Estimate	Standard Error
γ_{lat}	0.608	0.027
γ_{lon}	0.601	0.028
θ	0.027	0.019
$\Sigma_{lat,lon} / \sqrt{\Sigma_{lat,lat} \Sigma_{lon,lon}}$	-0.018	0.052
$\log \Sigma_{lat,lat}$	-9.189	0.114
$\log \Sigma_{lon,lon}$	-7.486	0.114

the seal was south of the 57.5°N parallel. Despite the southward drift, the seal then entered a large area of northward drift between 57.5°N and 63.5°N. North of the 63.5°N parallel, the latitudinal mean velocity field was estimated to have a southward attraction, keeping the seal close to the 63.5°N parallel. Further the model estimated an overall mean turning angle, θ . This parameter was estimated to be close to zero (Table 1), whereas both the latitudinal and longitudinal autocorrelation parameters were estimated to be close to 0.6.

Discussion

The GDCRW introduced here generalizes the DCRW movement model of Jonsen et al. (2005) in three ways. Firstly, whereas the DCRW handles irregular observations by linear interpolation in the observational model, the GDCRW allows modelling irregular observations directly in the movement process. Through this construction, time-scale corrections of the DCRW parameters were found by considering a time regular GDCRW. Secondly, the GDCRW generalizes the DCRW by allowing different auto-correlation parameters in the two coordinates. Hence, when the rotation parameter is zero, the GDCRW resembles the integrated velocity model of the CTCRW of Johnson et al. (2008). Like the CTCRW and

DCRW, the GDCRW includes the random walk as a limiting case. When the auto-correlation parameter approaches zero, the movement model approaches that of a random walk, which has been used in several studies, in particular when the data includes only daily observations (e.g. [Nielsen et al., 2006](#); [Lam et al., 2010](#)). Thirdly, the GDCRW extends the DCRW by including a drift term.

Including a drift term in the model is useful for animals moving persistently between areas, such as the ringed seal analysed in the case study. In the case study, the drift term was modelled by a location dependent field. Having location or time dependent parameters in the SDE greatly complicates the calculations to obtain an analytical solution and in turn a fully continuous time model. Therefore, location dependent mean velocities could not easily be implemented in the CTCRW which has previously been used to analyse the track ([Albertsen et al., 2015](#); [Thygesen et al., 2017](#)). Nonetheless, using the discrete time model, or a discrete time approximation, it is straightforward to extend the movement model with a location dependent drift. Using the same methods, spatial covariates such as sea surface temperature or depth could be included.

While the mean turning angle was estimated to be close to zero using the entire track, this may not be the case if, for instance, a time varying parameter or behavioural switching was included. Changes in behavioural states, $S_{t_i} \in \{1, 2, \dots, n\}$, can be modelled by a Markov Chain such that

$$P(S_{t_i} = k \mid S_{t_{i-1}} = j) = (\exp(Q\Delta_{t_i}))_{jk}$$

where Q is an $n \times n$ matrix such that $Q_{jk} > 0$ for $j \neq k$ and $Q_{jj} = -\sum_{\{k:j \neq k\}} Q_{jk}$. The movement model is modified to have different parameters depending on the current behavioural

state

$$X_{t_i} = X_{t_{i-1}} + \Delta_{t_i} \exp(-\Theta_{S_{t_i}} \Delta_{t_i})(X_{t_{i-1}} - X_{t_{i-2}})/\Delta_{t_{i-1}} + \Delta_{t_i} \left(I - \exp(-\Theta_{S_{t_i}} \Delta_{t_i}) \right) \mu_{S_{t_i}} + \Delta_{t_i} \epsilon_{t_i}.$$

This model generalizes the behavioural switching movement models of [Jonsen et al. \(2005\)](#) and [Whoriskey et al. \(2017\)](#). It assumes that switching only occurs at the predetermined time points; however, as it has been shown in both the case study and simulation studies, latent locations can be included either at regular time points, or at the time of observations and any time between them. While the extension to include behavioural switching is simple, maximum likelihood estimation is greatly complicated when measurement error is present.

The GDCRW can be constructed as a discretization of a generalization of the CTCRW. The first simulation study comparing the GDCRW and CTCRW suggests that using the analytical continuous time solution, when it can be found, generally provides better results than a discrete time approximation. Nonetheless, the discrete time approximation provided accurate parameter estimates, even when no additional latent states were included to improve the approximation. While the GDCRW was outperformed by the CTCRW in estimating true locations when the CTCRW was the true model, the first simulation study illustrated that the performance of the GDCRW could be improved to closely resemble the CTCRW by including additional latent states between observations.

The second simulation study compared the DCRW and the GDCRW in their ability to re-estimate the movement parameters of the underlying continuous time model. In both the tortuous and persistent movement scenarios, the GDCRW performed well; however, in the tortuous movement scenario, the performance was notably improved by adding additional

latent locations between observations. Further, it became evident that the parameter estimates of the DCRW are highly dependent on the selected time steps between latent locations. Nevertheless, the estimates could be corrected by equation (4): the GDCRW with regular time steps. This correction provided estimates close to the true values in all cases except in the tortuous movement case with 250 and 500 latent locations. Clearly, the ability to have time scale independent movement parameters is a key feature of the GDCRW, regardless of whether it is used with regular or irregular time steps. Time scale independent movement parameters allow analysis of several animals without using the same time steps, and further allow comparing results from previous studies using the DCRW even if different time steps are used.

Besides accuracy of the estimates, the DCRW and GDCRW were compared on their ability to reconstruct the movement tracks. The third simulation study showed that modelling time-irregular data through a time-irregular movement could increase the accuracy of predicted locations. This is consistent with previous findings comparing the DCRW and CTCRW, which showed that the continuous time model performed better if both movement models were combined with t-distributed measurement errors ([Albertsen et al., 2015](#)). Overall, using the GDCRW with irregular time steps performed well in both scenarios compared to the DCRW. For small measurement standard deviations, the irregular time steps outperformed the regular time steps with interpolation. For medium measurement standard deviations, the two approaches performed equally in the persistent movement scenario, whereas the DCRW slightly outperformed the GDCRW in the tortuous movement case. For large measurement standard deviations, the two approaches performed equally in both scenarios. Combined with the previous simulation study, these results suggest that having latent locations at the

time of observations generally performs well compared to the DCRW with equidistant time steps in the movement; keeping in mind that both improves as approximations to the same underlying continuous time movement model as the number of latent locations increases.

Directly modelling irregular data eases interpretation and comparison of movement parameters because they are scaled by the time steps. From equation (4), parameters of the DCRW and GDCRW can be transformed to any time scale. However, the simulation study shows that fitting the DCRW with a poorly chosen time step introduces bias. This poses a problem in population and meta studies. With a discrete time model, all animals must be fitted with the same time steps to compare movement parameters. However, if the same time step is not optimal for all animals, bias can be introduced. Using an irregular or continuous time model scales the parameters to a common time scale, even when the animals are observed, or behave, at different time scales.

References

- Albertsen, C. M. (2017). *covafillr: Local Polynomial Regression of State Dependent Covariates in State-Space Models*. R package version 0.4.1. <https://CRAN.R-project.org/package=covafillr>.
- Albertsen, C. M., Whoriskey, K., Yurkowski, D., Nielsen, A., and Flemming, J. (2015). Fast fitting of non-gaussian state-space models to animal movement data via template model builder. *Ecology*, 96(10):2598–2604, doi:10.1890/14-2101.1.
- Auger-Méthé, M., Albertsen, C. M., Jonsen, I. D., Derocher, A. E., Lidgard, D. C., Studholme,

- K. R., Bowen, W. D., Crossin, G. T., and Flemming, J. M. (2017). Spatiotemporal modelling of marine movement data using template model builder. *Marine Ecology Progress Series*, 565:237–249, doi:10.3354/meps12019. 0171-8630.
- Auger-Méthé, M., Field, C., Albertsen, C. M., Derocher, A., Lewis, M. A., Jonsen, I. D., and Flemming, J. M. (2016). State-space models’ dirty little secrets: even simple linear gaussian models can have parameter and state estimation problems. *Scientific Reports*, 6:26677, doi:10.1038/srep26677.
- Costa, D. P., Robinson, P. W., Arnould, J. P. Y., Harrison, A.-L., Simmons, S. E., Hassrick, J. L., Hoskins, A. J., Kirkman, S. P., Oosthuizen, H., Villegas-Amtmann, S., and Crocker, D. E. (2010). Accuracy of ARGOS locations of pinnipeds at-sea estimated using fastloc GPS. *PLoS ONE*, 5(1):e8677, doi:10.1371/journal.pone.0008677.
- Fournier, D. A., Skaug, H. J., Ancheta, J., Ianelli, J., Magnusson, A., Maunder, M. N., Nielsen, A., and Sibert, J. (2012). Ad model builder: using automatic differentiation for statistical inference of highly parameterized complex nonlinear models. *Optimization Methods and Software*, 27(2):233–249, doi:10.1080/10556788.2011.597854.
- Gentle, J. (2007). *Matrix Algebra: Theory, Computations, and Applications in Statistics*. Springer Texts in Statistics. Springer.
- Gurarie, E., Andrews, R. D., and Laidre, K. L. (2009). A novel method for identifying behavioural changes in animal movement data. *Ecology Letters*, 12(5):395–408, doi:10.1111/j.1461-0248.2009.01293.x.
- Hussey, N. E., Kessel, S. T., Aarestrup, K., Cooke, S. J., Cowley, P. D., Fisk, A. T., Harcourt,

- R. G., Holland, K. N., Iverson, S. J., Kocik, J. F., Mills Flemming, J. E., and Whoriskey, F. G. (2015). Aquatic animal telemetry: A panoramic window into the underwater world. *Science*, 348(6240), doi:10.1126/science.1255642.
- Johnson, D. S., London, J. M., Lea, M.-A., and Durban, J. W. (2008). Continuous-time correlated random walk model for animal telemetry data. *Ecology*, 89(5):1208–1215, doi:10.1890/07-1032.1.
- Jonsen, I. (2016). Joint estimation over multiple individuals improves behavioural state inference from animal movement data. *Scientific Reports*, 6:20625, doi:10.1038/srep20625.
- Jonsen, I. D., Flemming, J. M., and Myers, R. A. (2005). Robust state–space modeling of animal movement data. *Ecology*, 86(11):2874–2880, doi:10.1890/04-1852.
- Kristensen, K., Nielsen, A., Berg, C., Skaug, H., and Bell, B. (2016). Tmb: Automatic differentiation and laplace approximation. *Journal of Statistical Software*, 70(1):1–21, doi:10.18637/jss.v070.i05.
- Lam, C., Nielsen, A., and Sibert, J. (2010). Incorporating sea-surface temperature to the light-based geolocation model TrackIt. *Marine Ecology Progress Series*, 419:71–84, doi:10.3354/meps08862.
- McClintock, B. T., Johnson, D. S., Hooten, M. B., Ver Hoef, J. M., and Morales, J. M. (2014). When to be discrete: the importance of time formulation in understanding animal movement. *Movement Ecology*, 2(1):21, doi:10.1186/s40462-014-0021-6.
- McClintock, B. T., King, R., Thomas, L., Matthiopoulos, J., McConnell, B. J., and Morales,

- J. M. (2012). A general discrete-time modeling framework for animal movement using multistate random walks. *Ecological Monographs*, 82(3):335–349.
- Michélot, T., Langrock, R., and Patterson, T. A. (2016). moveHMM: an r package for the statistical modelling of animal movement data using hidden markov models. *Methods in Ecology and Evolution*, 7(11):1308–1315, doi:10.1111/2041-210x.12578.
- Morales, J. M., Haydon, D. T., Frair, J., Holsinger, K. E., and Fryxell, J. M. (2004). Extracting more out of relocation data: Building movement models as mixtures of random walks. *Ecology*, 85(9):2436–2445, doi:10.1890/03-0269.
- Nielsen, A., Bigelow, K. A., Musyl, M. K., and Sibert, J. R. (2006). Improving light-based geolocation by including sea surface temperature. *Fisheries Oceanography*, 15(4):314–325, doi:10.1111/j.1365-2419.2005.00401.x.
- Pedersen, M. W., Patterson, T. A., Thygesen, U. H., and Madsen, H. (2011). Estimating animal behavior and residency from movement data. *Oikos*, 120(9):1281–1290, doi:10.1111/j.1600-0706.2011.19044.x.
- Thygesen, U. H., Albertsen, C. M., Berg, C. W., Kristensen, K., and Nielsen, A. (2017). Validation of ecological state space models using the laplace approximation. *Environmental and Ecological Statistics*, 24(2):317–339, doi:10.1007/s10651-017-0372-4.
- Tracey, J. A., Zhu, J., and Crooks, K. R. (2010). Modeling and inference of animal movement using artificial neural networks. *Environmental and Ecological Statistics*, 18(3):393–410, doi:10.1007/s10651-010-0138-8.

Turchin, P. (1998). *Quantitative Analysis of Movement: Measuring and Modeling Population Redistribution in Animals and Plants*. Sinauer, Sunderland, MA, U.S.A.

Whoriskey, K., Auger-Méthé, M., Albertsen, C. M., Whoriskey, F. G., Binder, T. R., Krueger, C. C., and Flemming, J. M. (2017). A hidden markov movement model for rapidly identifying behavioral states from animal tracks. *Ecology and Evolution*, 7(7):2112–2121, doi:10.1002/ece3.2795.

Appendix S1: Solving the SDE

To solve the SDE,

$$dV_t = -\Theta(V_t - \mu)dt + SdB_t,$$

consider the process

$$Y_t = e^{\Theta t}(V_t - \mu)$$

Itô's formula yields

$$\begin{aligned} dY_t &= \Theta e^{\Theta t} V_t dt + e^{\Theta t} dV_t \\ &= \Theta e^{\Theta t} V_t dt + e^{\Theta t} (-\Theta(V_t - \mu)dt + SdB_t) \\ &= e^{\Theta t} SdB_t \end{aligned}$$

Hence,

$$e^{\Theta t}(V_t - \mu) = (V_0 - \mu) + \int_0^t e^{\Theta u} SdB_u$$

which implies

$$\begin{aligned} V_t - \mu &= e^{-\Theta t}(V_0 - \mu) + e^{-\Theta t} \int_0^t e^{\Theta s} SdB_s \\ &= e^{-\Theta t} V_0 + (I - e^{-\Theta t}) \mu + \int_0^t e^{-\Theta(t-s)} SdB_s \end{aligned}$$

Since this is a sum of a deterministic term and an integral of a deterministic function with respect to a Wiener process with Gaussian increments, the distribution is Gaussian. The mean of the increment is

$$\begin{aligned} E(V_t | V_0) &= E\left(e^{-\Theta t} V_0 + (I - e^{-\Theta t}) \mu | V_0\right) + E\left(\int_0^t e^{-\Theta(t-s)} SdB_s | V_0\right) \\ &= e^{-\Theta t} V_0 + (I - e^{-\Theta t}) \mu \end{aligned}$$

Using Itô isometry, the variance is

$$\begin{aligned}
Var(V_t | V_0) &= Var\left(e^{-\Theta t}V_0 + (I - e^{-\Theta t})\mu + \int_0^t e^{-\Theta(t-s)}SdB_s \mid V_0\right) \\
&= Var\left(\int_0^t e^{-\Theta(t-s)}SdB_s \mid V_0\right) \\
&= Var\left(\int_0^t e^{-\Theta(t-s)}SdB_s\right) \\
&= E\left(\left(\int_0^t e^{-\Theta(t-s)}SdB_s\right)^2\right) - E\left(\int_0^t e^{-\Theta(t-s)}SdB_s\right)^2 \\
&= E\left(\left(\int_0^t e^{-\Theta(t-s)}SdB_s\right)^2\right) \\
&= \int_0^t e^{-\Theta(t-s)}SS^T\left(e^{-\Theta(t-s)}\right)^T ds \\
&= \int_0^t e^{-\Theta(t-s)}\Sigma\left(e^{-\Theta(t-s)}\right)^T ds
\end{aligned}$$

Now ([Gentle, 2007](#)),

$$\begin{aligned}
\text{vec}(Var(V_t | V_0)) &= \int_0^t e^{-\Theta(t-s)} \otimes e^{-\Theta(t-s)} \text{vec}(\Sigma) ds \\
&= \int_0^t e^{-\Theta \oplus \Theta(t-s)} ds \text{vec}(\Sigma) \\
&= (\Theta \oplus \Theta)^{-1} (I - e^{-\Theta \oplus \Theta t}) \text{vec}(\Sigma)
\end{aligned}$$

where \oplus denotes the Kronecker sum, $A \oplus B = A \otimes I_B + I_A \otimes B$.

Defining the matrix C such that $\text{vec}(C) = (\Theta \oplus \Theta)^{-1} \text{vec}(\Sigma)$,

$$\begin{aligned}
\text{vec}(Var(V_t | V_0)) &= (\Theta \oplus \Theta)^{-1} \text{vec}(\Sigma) - (\Theta \oplus \Theta)^{-1} e^{-\Theta \oplus \Theta t} \text{vec}(\Sigma) \\
&= (\Theta \oplus \Theta)^{-1} \text{vec}(\Sigma) - e^{-\Theta \oplus \Theta t} (\Theta \oplus \Theta)^{-1} \text{vec}(\Sigma) \\
&= \text{vec}(C) - e^{-\Theta \oplus \Theta t} \text{vec}(C) \\
&= \text{vec}(C) - e^{-\Theta t} \otimes e^{-\Theta t} \text{vec}(C)
\end{aligned}$$

Hence,

$$\text{Var}(V_t | V_0) = C - e^{-\Theta t} C e^{-\Theta^T t}$$

Appendix S2: Simulation method details

To simulate from the process,

$$dV_t = -\Theta(V_t - \mu)dt + SdB_t dX_t = V_t dt$$

time steps, $\Delta_{t_i} = t_i - t_{i-1}$, between observations were simulated from a mixture of an exponential distribution and a normal distribution. To simulate from the mixture, a uniform random variable, $U \sim \text{unif}(0, 1)$, an exponentially distributed random variable, $\delta_0 \sim \text{exp}(1)$, and a Gaussian random variable, $\delta_1 \sim N(10, 0.5^2)$, were simulated. Then the time step was

$$\Delta_{t_i} = \begin{cases} 0.1 + \delta_0 & U < 0.9 \\ 0.1 + \max(\delta_1, 0.01) & U \geq 0.9 \end{cases}$$

The resulting density function is seen in [Fig. 7](#).

Between two time points t_i and t_{i+1} , the processes were simulated using the Euler-Maruyama approximation,

$$V_{s(j+1)} = V_{s(j)} - \Theta(V_{s(j)} - \mu)\Delta_{s(j+1)} + S\eta_{s(j+1)}X_{s(j+1)} = X_{s(j)} + V_{s(j+1)}\Delta_{s(j+1)}$$

with $s(j) = t_i + (n)/199 \cdot \Delta_{t_{i+1}}$, $j = 0, 1, \dots, 199$. Simulated examples can be seen in [Fig. 8](#)

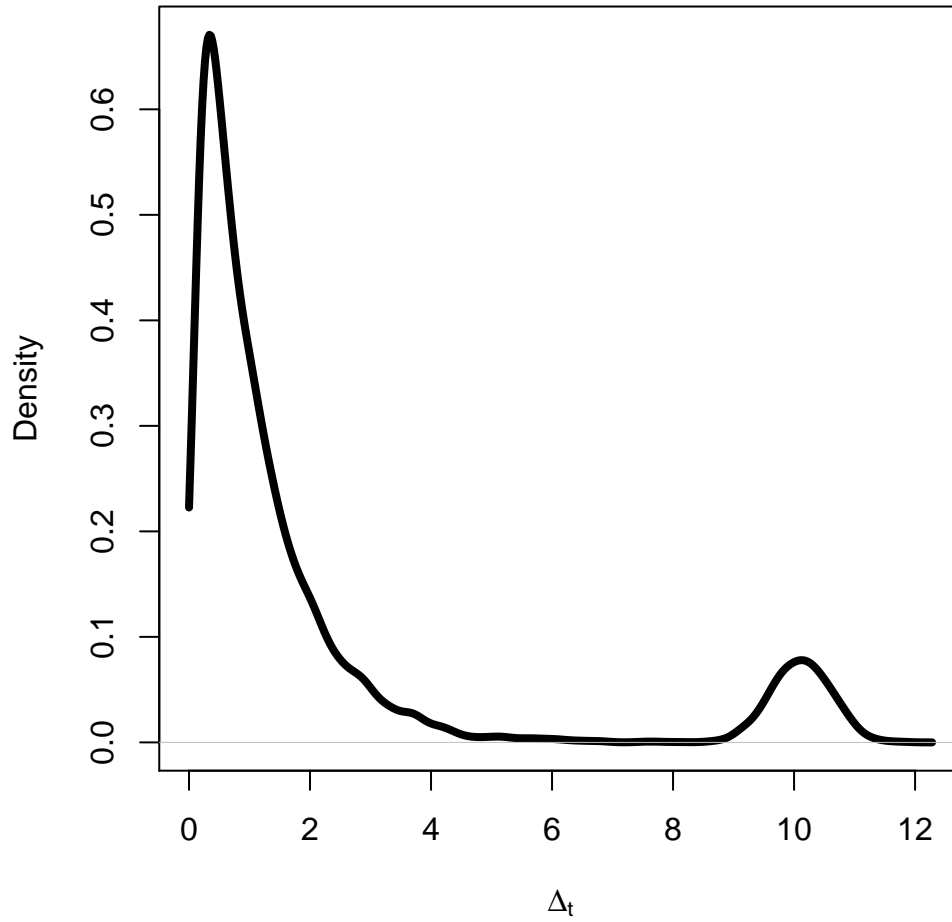


Fig. 7: Probability density function used to simulate time steps.

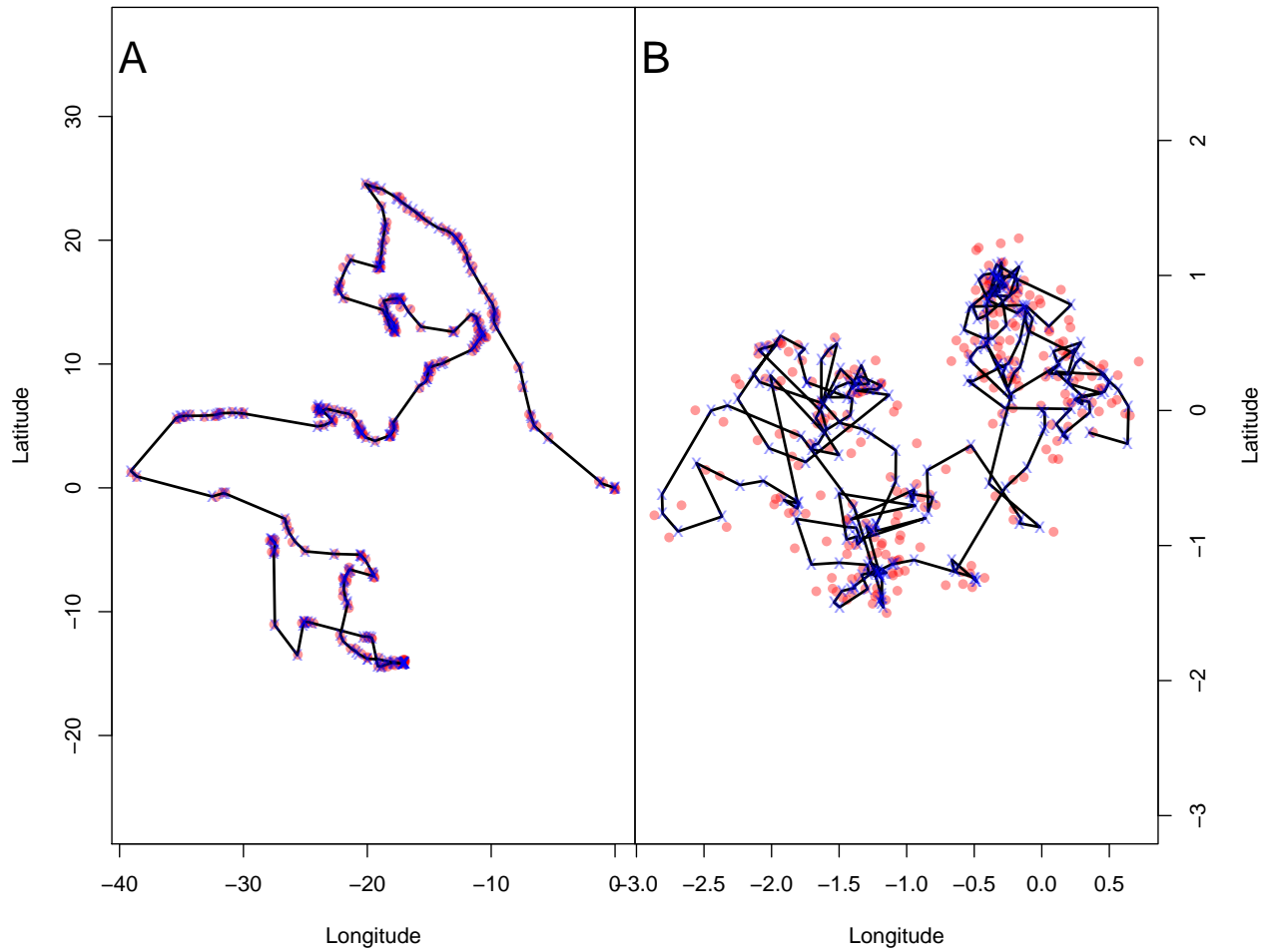


Fig. 8: Simulated trajectories (blue crosses connected by black lines) and observations (red points) from the SDE model in the two scenarios: persistent (A) and tortuous (B) movement.